

Chapter 7

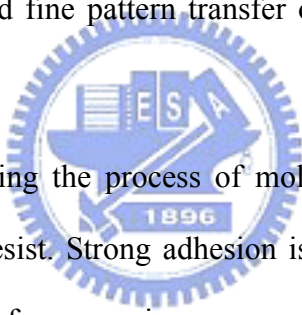
Effect of Fluoroalkyl Substituents for the Reaction of Alkylchlorosilanes on Silicon Oxide Surfaces for Nanoimprint

Abstract

As all imprint techniques rely on contact between resist and mold, the wetting and adhesion characteristics of the polymer materials to the substrate are critical issues. The strength of adhesion between mold surface and resist is characterized by the amount of energy required to separate the two materials. In this study, trichloro(3,3,3-trifluoropropyl)silane (FPTS) and trichloro(1H, 1H, 2H, 2H-perfluorooctyl)silane (FOTS) are used for self-assembled monolayers (SAM) on mold (SiO_2/Si) as releasing and anti-sticking layers for nanoimprint. Chemical reaction between the head groups of different fluorinated trichlorosilanes and the surface hydroxyl groups by FTIR. The SAM quality depends on immersion time and silanization temperature that were investigated through measurement of the ellipsometer and calculation of the surface energy. It has been demonstrated that less defect and lower roughness of the resist surface can be achieved by mold with SAMs of FOTS and FPTS. The mold with FOTS layer processes lower surface energy (8 mJ/m^2) and smoother of the resist after imprinting. The surface energy of the SAM on mold (SiO_2/Si) dictates the resulted in quality of better resist surface and the pattern formation.

7.1 INTRODUCTION

The application of nanofabrication to printing gives rise to a need to develop a competitive parallel process, which may serve the technological demands of nanoelectronics and related areas, while bearing in mind reliability, throughput and cost. Thermal nanoimprint lithography is a promising method to fabricate integrated fine patterns using various materials. [1] In thermal nanoimprint lithography, a thermoplastic polymer is heated above its glass transition temperature (T_g), and a fine mold is pressed on the polymer. After cooling down below its T_g , the mold is released and the fine pattern on the mold is transferred to the polymer. Using thermal nanoimprint processes, fabrication of high aspect ratio patterns,[2] curved cross-sectional patterns,[3] and fine pattern transfer on novel plastic plates,[4] have been reported.



Stickiness is present during the process of mold release after thermal contact between mold and polymer resist. Strong adhesion is generally caused by capillary, electrostatic, van der Waals force, or in some cases by hydrogen bonding. To overcome the adhesion problem, a self-assembled monolayer (SAM) formation can be used to modify the surface property which becomes important in surface science, molecular recognition, electrochemistry, microelectronic engineering, nanotechnological structures, bioactive surfaces, and many other fields. In practice, one of the most commonly used SAM is the organosilane monolayer on hydroxyl surface such as silica, sapphire, or oxidized silicon. While techniques such as contact angle measurement,[5] ellipsometry,[6] UV-vis spectroscopy,[7] FTIR spectroscopy,[8] ESCA at variable angles,[9] X-ray,[10] AFM,[11,12] and STM [13] have been applied to characterize the organosilane SAM surface. However, very little is known concerning the detailed formation process. Therefore, the treatment of the mold

surface with a fluorine monolayered polymer has been introduced to decrease the surface energy of the mold and minimize charge trapping. [4, 14]

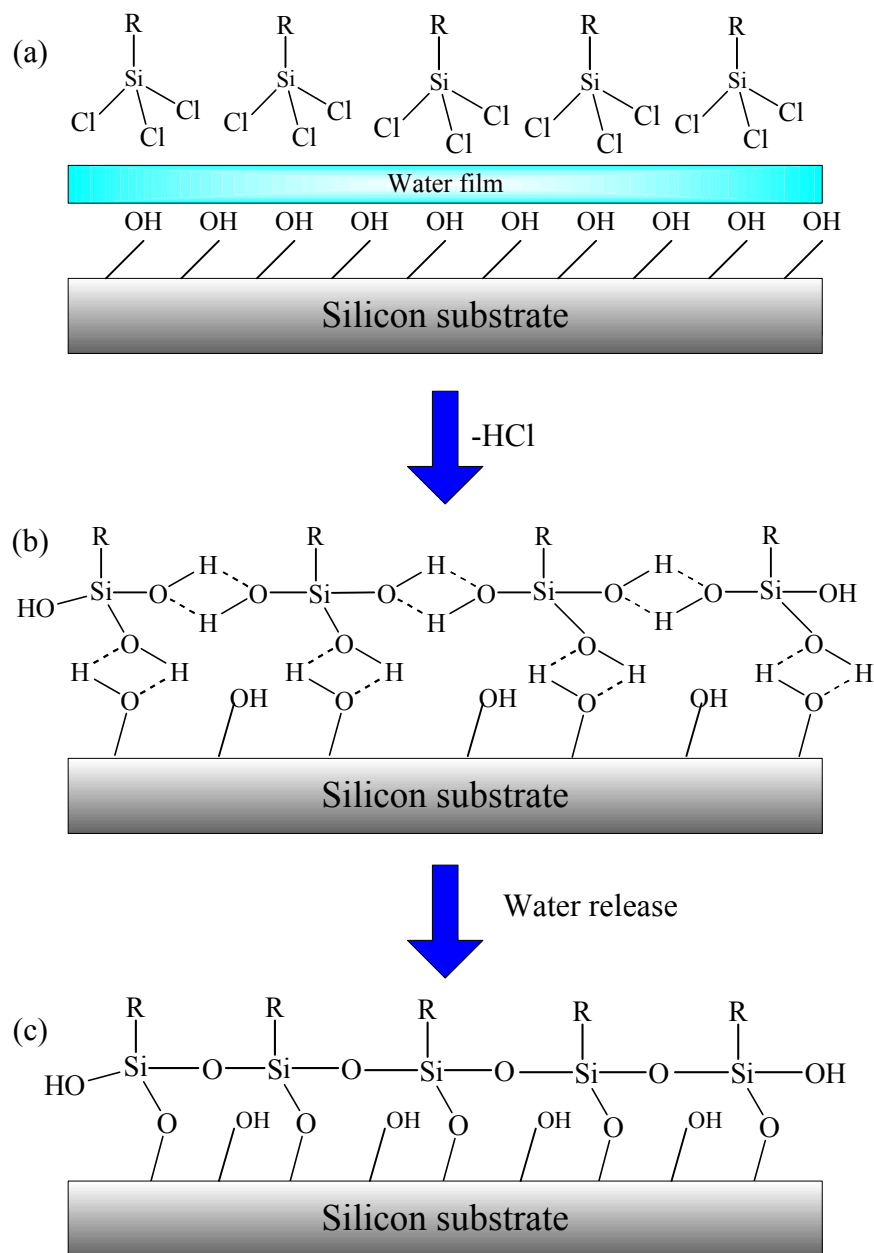
Due to the covalent nature of SAM formation, it is convenient to assume that the SAM formation is a 1:1 reaction between the monolayer and surface. AFM studies revealed that the surface of SAM/silica is always smoother in topography than the bare silica surface. Although AFM provides valuable information about the SAM surface topography, it still does not provide the detailed chemical mechanism of SAM formation. Organosilane SAM formation on silica/silicon is believed to be accomplished through surface adsorption/hydration/silanization.[15] In the process, the silanol (SiOH) groups on the glass are believed to react with either R-SiCl₃ or R-Si(O(CH₂)_n-CH₃)₃ through a dehydration process and thus form strong chemical bonds. The roughness for pattern fabrication by nanoimprint lithography during the mold release process is caused the undesirable deformation of the resist. In this chapter, the formation process of SAM is investigated through the calculation of surface energy. The morphology of the polymer resist surface pattern after thermal nanoimprint can be used to evaluate the surface roughness and resolution of patterns.

7.2 EXPERIMENTAL

7.2.1 SAM Film Formation

Trichloro(3,3,3-trifluoropropyl)silane (FPTS) and trichloro(1H, 1H, 2H, 2H-perfluorooctyl)silane (FOTS) were used as precursors for SAM on the mold as the mold releasers and anti-sticking layers for nanoimprint. Both FPTS and FOTS were purchased from Aldrich and used as received. Two SAM coating processes have been developed and demonstrated for nanoimprint applications. One is based on trichloro(3,3,3-trifluoropropyl)silane (FPTS), and the other on trichloro(1H, 1H, 2H,

2H- perfluorooctyl)silane (FOTS). Layer formation proceeds in the following three steps as illustrated in Scheme 7-1: (a) physical adsorption of the SAM to the previously formed water film on the silicon oxide substrate, (b) hydration of the chlorosilane groups where the Cl atoms are exchanged by OH groups by reacting with water to release HCl, and (c) polymerization of the SAM at the surface where the



Scheme 7-1. Layer formation process in the three steps.

siloxane molecules become linked together laterally via O atoms by releasing water. Process of SAM coating or silanization on silicon using the RSiCl_3 precursor begins with the hydrolysis of the polar head-groups and converts Si-Cl to Si-OH (silanol) end-groups [17,18]. The silicon wafer was immersed in a 1% solution of FPTS or FOTS in toluene for 1 hour then rinsed by pure toluene to remove excess silane. These species strongly attached to the hydrophilic surface of the oxidized silicon were annealed at about 150°C for 30 min to condense and react with silanol of other precursor molecules and the silanol on the surface to produce covalent siloxane bond, Si-O-Si.

7.2.2 SAM Films Analysis

FTIR (Bio-Rad, Model FTS-40, MASS, USA) was used to evaluate the structural change of the SAM after annealing at 150°C for 2 hours of the mold with the pattern. Surface properties of the SAM were examined by the contact angle measurement. An accurate thickness measurement by an ellipsometer (SOPRA SE-5, SOPRA, French) of the SAM is able to provide evidence of monomer layers formation without excess silane. The advancing and receiving contact angles of water, glycol and di-iodomethane were measured by increasing the water drop volume using a contact angle goniometer (GH100, Kruss, Germany). The surface roughness and micro-scale profile were measured using an atomic force microscope (AFM, Digital Instruments, DI-5000, USA).

7.2.3 Optical Ellipsometry

Ellipsometer (SOPRA SE-5, SOPRA, French) operating at the range of 300~800 nm at a 75° angle of incidence was used with a beam spot of 2 mm. Measurements

were made at three different spots for each sample. The phase shift and amplitude ratio ellipsometric parameter, Δ and Ψ [19], were determined from the observed polarizer and analyzer angles. The instrumental precision of the ellipsometric angle is 0.04° , and the sample-to-sample error in terms of final calculated FPTS or FOTS film thicknesses is within $\pm 1 \text{ \AA}$. The time of a single measurement was approximately 3 min, and the complete set of multiple measurements for each bare substrate was within 10 min after precleaning. In the calculation of the FPTS or FOTS film thicknesses, the optical response of FPTS or FOTS layer can be treated with two limiting models: (1) isotropic and (2) anisotropic. The details of the calculations in the isotropic approximation have been reported previously.[20, 21]

7.2.4 Surface Energy Calculations

Contact angle was measured using a Kruss-G40 Contact Angle Goniometer. Surface energy was evaluated using the Lifshitz-van der Waals acid-base approach (three liquid acid-base method) that has been proposed by van Oss et al. [22,23] This methodology introduces new meanings for the concept of “apolar” (Lifshitz-van der Waals, γ^{LW}) and “polar” (Lewis acid-base, γ^{AB}), the latter cannot be represented by a single parameter such as γ^p . Briefly, the theoretical approach follows the additive concept previously suggested by Fowkes.[24]

$$\gamma = \gamma^d + \gamma^{AB} \quad (1)$$

where γ^d stands for the dispersive term of the surface tension. The superscript AB refers to acid-base interaction. By regrouping components in eq (1), van Oss et al. expressed the surface energy as

$$\gamma = \gamma^{LW} + \gamma^{AB} \quad (2)$$

In addition, two parameters were created to describe the strength of the Lewis acid and base interactions:

γ_s^+ =(Lewis) acid parameter of surface free energy

γ_s^- =(Lewis) base parameter of surface free energy

$$\gamma^{AB} = 2(\gamma_s^+ \gamma_s^-)^{1/2} \quad (3)$$

van Oss, Good, and their co-workers developed a “three-liquid procedure” (eq 4) to determine γ_s by the contact angle technique.

$$\gamma_L(1 + \cos \theta) = 2 \left[(\gamma_s^{LW} \gamma_L^{LW})^{1/2} + (\gamma_s^+ \gamma_L^-)^{1/2} + (\gamma_s^- \gamma_L^+)^{1/2} \right] \quad (4)$$

To determine the components of γ_s of a polymer solid, three liquids are selected, two of them are polar and the third one is apolar. The polar pairs, water and ethylene glycol, and water and formamide, are employed to give good results. The apolar liquid is either diiodomethane or R-bromonaphthalene because the LW, parameters of the Lewis acid and the Lewis base are available. Parameters of γ_s of Lewis acid and the Lewis base can then be determined by solving these three equations simultaneously from eq.(3)-eq.(4). By measuring contact angles of water, diiodomethane, and ethylene glycol, γ_L^{LW} , γ_L^+ and γ_L^- can be obtained [25-27].

7.2.5 Nanoimprint Process

The resist, 22A4, was purchased from the Sumitomo Chemical Company for nanoimprint. The combination of resist and mold surface modification has been successfully demonstrated using an imprint tool developed by Nanonex (nx-1000, US). The mold has a size of 1 X 1 cm² containing test structure with a depth of 240 nm consisting of lines and dots. The resist contact between and mold was under

preprint pressure of 200 psi at preprint temperature of 110 °C, then an imprint force of 380 psi was used to press the mold into a 300-nm thick resist with a duration of 5 min at 130 °C.

7.3 RESULTS AND DISCUSSION

7.3.1 *Functional Groups of SAM*

The formation of the SAM layer can be verified by FTIR measurements when the hydrolyzed silica surface remains nearly unchanged during SAM formation, only a few fractions of surface bonds are formed. Figure 7-1 shows the FTIR spectra of the reaction products of FOTS and FPTS with the hydrated silica at room temperature following by annealing at 150°C for 2 hours. Hydrolysis of the silane with surface water occurs based on the disappearance of the H₂O deformation mode at 1618 cm⁻¹ and the formation of HC1 (not shown). Both bonds at 3347 cm⁻¹ (SiO-H) and 985 cm⁻¹ (Si-OH) disappeared due to the alkylsilanol [28]. The appearance at 588 and 490 cm⁻¹ are due to the weak Si-C1 bond from the parent compound [29]. By using the spectrum of the silica as a reference, the negative bonds produced in the absorbance spectra are due to bonds being removed from the silica while the positive bonds are due to bonds formed on the surface. The negative bond at 3747 is due to the SiO-H stretching mode of the isolated geminal surface silanols and its disappearance indicates the interaction of the surface Si_sOH groups (Si_s refers to a surface silicon atom.) and the alkylsilanol as shown in Figure 7-1. The key spectral region used to differentiate between these possibilities is the Si-O-Si bond at 1060 cm⁻¹. The Si-O-Si bond may come from reactions between the surface Si_s-OH groups, the cross-linking between adjacent alkylsilanols, and the polymerization products depositing on the surface. Other bonds located at 2800 cm⁻¹ and those between 1450 and 700 cm⁻¹ are

attributed to various C-F and C-H modes.

7.3.2 Thickness Analysis

In Figure 7-2, the ellipsometric thickness is plotted as functions of silanization temperatures. Two curves shown represent the thickness based on a specific ideal limiting structure of FPTs and FOTS layers, respectively. The SAM is considered to consist of the conformation of ally disordered chains with no directional dependence before silanization. The thickness of the SAM decreases with the increase of the silanization temperature due to conformation of more uniform and the densest-packed ensemble of alkyl chains, resulting in decrease of the thickness of the SAM. The thicknesses of SAMs are closed to constant values determined as 1.11 and 1.4 nm for FPTs and FOTS respectively when the silanization temperature is above 150°C. The FPTs with lower fluorosiloxane content results in higher silanization temperature dependence ascribed to the shorter alkyl chains for regular package. This observation implies that the FPTs coverage is closer to the anisotropic case. In the FOTS case, the higher fluorosiloxane content results in an ensemble of conformationally disordered chains with no directional dependence, implying that the FOTS coverage is closer to the isotropic case.

7.3.3 Contact Angle and Surface Free Energy

Plots of surface free energy as a function of immersion time at 150 °C of the silanization temperature are displayed in Figure 7-3, showing two distinct regimes. The surface energies of the SAMs for FOTS and FPTs decrease rapidly as the silanization time is below 10 min. This observation indicates that most of the silanization reaction takes place within the first 10 min. The surface free energy tends

to approach to a constant after 10 min of immersion time, implying the completeness of the silanization reaction. Plots of silanization temperature as a function of surface energy on two sets of samples prepared for 30 min of immersion time are given in Figure 7-4. The surface energy of SAM decreases with the increase of silanization temperature. SAM surface free energies of FPTS and FOTS tend to approach to constant values determined as 14.1 and 8.2 mJ/m² respectively when the silanization temperature is above 120°C.[30-32] The SAM of FOTS with higher fluorosiloxane content resulted in the lower surface energy.

The hysteresis in the contact angle measurements was determined from the equation $\delta = |\cos(\theta_a) - \cos(\theta_r)|$, [33] where θ_a and θ_r are advancing and receding contact angles, respectively. The average value of δ for all investigated liquids on the silanized wafer was found to be a temperature-independent value at 0.037 ± 0.05 as listed in Table 7-1. At low silanization temperatures, higher value of hysteresis is obtained. Furthermore, the phenomenological model [34] suggests that the hysteresis contact angle is due to the presence of chemical or physical heterogeneities and/or slow surface reorganization (surface dynamics). On this basis, some qualitative inferences can be made. Below 75°C of silanization temperature with high hysteresis value and unstable structure, the formation of disorganized monolayer is observed. Above 75°C, the low hysteresis value observed is consistent with the formation of densely-packed monolayer with a more uniform surface. In addition, the FPTS layer with lower fluorosiloxane content resulted in smaller hysteresis (δ), ascribed to the shorter alkyl chains reorganized easily to form dense-packed structure.

Silanization at room temperature results in higher surface free energy due to the present of the hydroxyl group from the hydrolysis of FPTS and FOTS. Lewis base and acid components (γ^- , γ^+) of surface energies determined in this study are listed in

Table 7-2. The Lewis-acid component (γ^+) of surface energy is close to zero after the silanization reaction, which leads to a vanishing value of the donor-acceptor component. According to Good and van Oss,[35] the mild ability of the higher fluorosiloxane content (FOTS) to accept electron pairs is due to the polarization as a result of the strong inductive effect relayed by the fluorocarbon chain. The Lewis-base component (γ_s^-) is quite well defined in all cases, reflecting the presence of nonbonded electron pairs on the SAM.

7.3.4 Surface Topography

Figure 7-5 shows AFM micrographs of SAMs for silanization temperature at 150°C. These AFM micrographs indicate that these layer surfaces quite smooth for both SAMs. The SAM images of FPTs and FOTS are virtually featureless, with root mean square roughness of about 0.468 and 0.189 nm, respectively. With lower fluorosiloxane content, the AFM image shows a larger number of bright spots, corresponding to small patches of the film which are typically 10-15 Å thick and less than 40 Å in diameter [36, 37]. The FPTs with lower fluorosiloxane chains results in larger number of bright spots. SAM image containing higher fluoroalkyl chain (FOTS) results in lower roughness and less number of bright spots. Therefore, the surface with FOTS has fewer defects than that of the FPTs characterized by AFM.

In nanoimprinting, the transfer of pattern from mold to the resist on the substrate requires antiwetting surface of the mold to minimize the defects induced by strains. Figure 7-6 shows AFM micrographs of the surface resist after separation from the mold with SAMs of FPTs and FOTS under a typical process temperature of 200°C and typical pressure of 100 bar. The root mean square roughness of the resist surface after separation from mold with the surface of silicon oxide surface, FPTs and FOTS

monolayers are 1.568, 0.369 and 0.131 nm, respectively.

Figure 7-7 shows the scanning electron micrograph (SEM) images of the isolated trench transferred by imprint with width of 120 and 60 nm after separation from the mold of silicon oxide surface and SAMs of FPTs and FOTS. The physical and mechanical adhesions between the mold and the silicon oxide surface result in the formation of defects during separation of the mold from the resists. Furthermore, stickiness between silicon oxide surface and resist causes the deformation of the imprint pattern during the process of separation as shown in Figure 7-7 (a). The defect caused by the stickiness is reduced by using the mold with SAMs of FPTs and FOTS as shown in Figures 7 (b) and 7 (c). The best trench was fabricated by using the mold with FOTS, suggesting that lower surface free energy indeed decreases the stickiness between mold and resist and enhances the imprint quality.

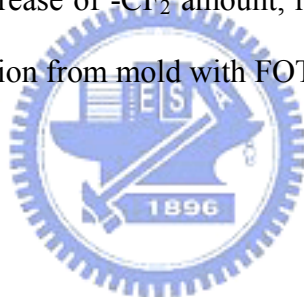
7.3.5 Stability of FPTs and FOTS

To investigate the stability of the SAMs for plasma, acid and base resistance, FOTS and FPTs layers have been tested through oxygen plasma, 0.1 N HCl and NaOH solutions for a series of time. Contact angles of water on the FPTs and FOTS surfaces after oxygen plasma treatment for a series of time are shown in Figure 7-8. The contact angles of water for FPTs and FOTS monolayers without plasma treatment are 86° and 111°, respectively. Both contact angles of water decrease rapidly to 10° after only 10 sec of oxygen plasma treatment and remain nearly constant thereafter. This observation suggests that oxygen plasma is able to decompose both of FPTs and FOTS layers completely, implying that the antiwetting properties of FPTs and FOTS can be eliminated by oxygen plasma treatment for about 10 sec. In addition, the acid and base resistances have been tested through immersion in 0.1 N HNO₃ and NaOH

solutions for a series of time at 100°C. Surface energy parameters calculated by advancing contact angles for water, diiodomethane (DIM) and ethylene Glycol (EG) water are listed in Table 7-3 and Table 7-4. The results suggest that both SAMs form FOTS and FPTS process excellent properties of acid and base resistances.

7.4 CONCLUSIONS

The SAMs of fluoroalkyl substituents on silicon oxide surfaces for nanoimprint reduce the physical and chemical adhesion between mold (SiO₂/Si) and resists. The higher fluorosiloxanes with longer flexible chain reduced the roughness of the resists after separation from mold due to the lower mechanical adhesion. The total surface energy decreased with the increase of -CF₂ amount, resulting in the optimum pattern of isolated trench after separation from mold with FOTS monolayer.



REFERENCES

1. S. Y. Chou; P. R. Krauss; P. J. Renstrom. *Appl. Phys. Lett.* **67**, 3114 (1995).
2. Y. Hirai; T. Yoshikawa; N. Takagi; S. Yoshida; K. Yamamoto. *J. Photopolym. Sci. Technol.* **16**, 615 (2003).
3. Y. Hirai; S. Harada; H. Kikuta; Y. Tanaka; M. Okano; S. Isaka; M. Kobayasi. *J. Vac. Sci. Technol. B*, **20**, 2867 (2003).
4. Y. Hirai; N. Takagi; S. Harada; Y. Tanaka. *Sens. Micromach. Soc.* **122**, 404 (2002).
5. N. Tillman; A. Ulman; J. S. Schildkraut; T. L. Penner. *J. Am. Chem. Soc.*, **110**, 6136 (1988).
6. A. N. Parikh; D. L. Allara; I. B. Azouz; F. Rondelez. *J. Phys. Chem.*, **98**, 7577 (1994).
7. K. Mathauer; C. W. Frank. *Langmuir*, **9**, 3446 (1993).
8. J. D. Le Grange; J. L. Markham. *Langmuir*, **9**, 1749 (1993).
9. L. B. Hazell; I. S. Brown; F. Freisinger. *Surf. Interface Anal.*, **8**, 25 (1986).
10. S. R. Wasserman; G. M. Whitesides; I. M. Tidswell; B. M. Ocko; P. S. Pershan; J. D. Axe. *J. Am. Chem. Soc.*, **111**, 5852 (1989).
11. V. V. Tsukruk; D. H. Reneker. *Polymer*, **36**, 1791 (1995).
12. F. K. Perkins; E. A. Dobisz; S. L. Brandow; T. S. Koloski; J. M. Calvert; K. W. Rhee; J. E. Kosakowski; C. R. K. Marrian. *J. Vac. Sci. Technol. B*, **12**, 3725 (1994).
13. J. L. Wilbur; H. A. Biebuyck; J. C. MacDonald; G. M. Whitesides. *Langmuir*, **11**, 825 (1995).
14. H. Scheer; H. Schultz; T. Holffmann; C. Torres. *J. Vac. Sci. Technol. B* **16**, 3917 (1998).
15. P. Silberzan; L. Leger; D. Ausserre; J. J. Benattar. *Langmuir*, **7**, 1647 (1991).
16. A. N. Parikh; D. L. Allara; I. B. Azouz; F. Rondelez. *J. Phys. Chem.* **98**, 577 (1994).

17. R. G. Good; C. J. van Oss. In *Modern Approaches to Wettability: Theory and Applications*; M. E. Schrader, G. Loeb. Plenum Press: New York. 1 (1991).
18. R. G. Good; M. K. Chaudhury; C. J. van Oss. In *Fundamentals of Adhesion*; L. H. Lee, Ed.; Plenum Press: New York. 153 (1991).
19. (a) R. M. A. Azzam; N. M. Bashara. *Ellipsometry and Polarized Light*; North-Holland: Amsterdam, The Netherlands (1977) (b) D. E. Aspnes. In *Optical Properties of Solids: New Developments*; North-Holland: Amsterdam, The Netherlands (1976); Chapter 15. (c) P. Yeh. *Optical Waves in Layered Media*; Wiley-Interscience: New York, (1988).
20. D. L. Allara; R. G. Nuzzo. *Langmuir*, **1**, 52 (1987).
21. S. R. Wasserman; G. M. Whitesides; I. M. Tidswell; B. M. Ocko; P. S. Pershan; J. D. Axe. *J. Am. Chem. SOC.*, **111**, 5852 (1989).
22. C. J. van Oss; M. K. Chaudhury; R. J. Good. *Chem. Rev.*, **88**, 927 (1988).
23. C. J. van Oss; L. Ju; M. K. Chaudhury; R. J. Good. *J. Colloid Interface Sci.*, **128**, 313 (1989).
24. F. M. Fowkes. *J. Phys. Chem.*, **66**, 382 (1962).
25. G. W. C. Kaye, T. H. Laby. Eds. *Table of Physical and Chemical Constants*, 15th ed.; Longman Scientific and Technical: Harlow (1992).
26. D. R. Lide, Ed. *Handbook of Chemistry and Physics*, 76th ed.; CRC Press (1995).
27. C. J. Drummond; D. Y. C. Chan. *Langmuir*, **13**, 3890 (1997).
28. C. P. Tripp; M. L. Hair. *J. Phys. Chem.*, **97**, 5693 (1993).
29. C. P. Tripp; M. L. Hair. *Langmuir*, **7**, 923 (1991).
30. S. R. Wasserman; Y. T. Tao; G. M. Whitesides. *Langmuir*, **5**, 1074 (1989).
31. P. Silberzan; L. Leger; D. Aussere; J. J. Benattar. *Langmuir*, **7**, 1647 (1991).
32. J. B. Brzoska; N. Shahidzadeh; F. Rondelez. *Nature*, **360**, 719 (1992).
33. R. J. Good. *J. Am. Chem. SOC.* **74**, 5041 (1952). (b) M. Morra; E. Occhiello; F.

- Garbassi. *Adv. Colloid Interface Sci.* **32**, 79 (1990).
34. (a) L. W. Schwartz; S. Garoff. *Langmuir*, **1**, 219 (1985). (b) J. F. Joanny; P. G. deGennes. *J. Chem. Phys.*, **81**, 552 (1984).
35. R. J. Good. In *Contact Angle, Wettability, and Adhesion*; VSP: Utrecht, The Netherlands (1993).
36. F. Fan; C. Maldarelli; A. Couzis. *Langmuir*, **19**, 3254 (2003).
37. P. A. Heiney; G. Kirsten; J. Fang. *Langmuir*, **16**, 2651 (2000).



Table 7-1 (a) Hysteresis calculated from advancing contact angles and receding angles for Water, Diiodomethane (*DIM*) and Ethylene Glycol (*EG*) on (a) FPTS and (b) FOTS monolayers as function of anneal time for monolayers formation.

(a)

Anneal temperature(°C)	Contact angle	water	δ_w	glycerol	δ_g	diiodomethane	δ_d
23	advancing angle	75.3± 1.7	0.226	74.7 ±2.3	0.201	80.5 ±2.3	0.219
	receding angle	61.3±1.8		62.3±1.7		67.4±2.1	
50	advancing angle	84.8 ±1.9	0.300	82.7±2.1	0.211	84.8±1.9	0.217
	receding angle	67.0±1.7		70.2±2.5		72.1±1.7	
75	advancing angle	92.3 ±1.8	0.329	88.8±1.9	0.228	88.2±1.9	0.187
	receding angle	73.2±1.6		75.6±1.9		77.4±2.5	
100	advancing angle	96.1 ±1.7	0.168	91.6±2.3	0.207	90.6 ±2.3	0.192
	receding angle	86.5±1.9		79.7±2.1		79.6±1.7	
125	advancing angle	97.6±1.8	0.171	93.4±2.0	0.185	91.8 ±1.9	0.179
	receding angle	87.8±2.0		82.8±1.9		81.5±1.5	
150	advancing angle	98.6±1.9	0.172	94.9±1.9	0.188	92.9 ±1.4	0.174
	receding angle	88.7±1.5		84.1±1.5		82.9±1.6	
175	advancing angle	99.4±1.6	0.173	96.2±1.7	0.182	93.3 ±1.5	0.169
	receding angle	89.4±1.8		85.7±1.6		83.6±1.5	
200	advancing angle	98.7±1.7	0.173	97.0±1.6	0.171	93.2 ±1.4	0.165
	receding angle	88.8 ±1.6		87.2±1.4		83.7±1.5	

(b)

Anneal temperature(°C)	Contact angle	water	δ_w	glycerol	δ_g	diiodomethane	δ_d
23	advancing angle	71.1± 1.7	0.275	73.3 ±2.5	0.299	82.0 ±2.5	0.280
	receding angle	53.2± 2.2		54.1±2.1		65.2±2.6	
50	advancing angle	82.5 ± 2.1	0.328	83.5±2.3	0.294	87.7±2.5	0.299
	receding angle	62.7±2.3		66±2.4		70.1±2.3	
75	advancing angle	92.8±2.6	0.344	95.5±2.0	0.313	101.3±2.4	0.277
	receding angle	72.9±2.0		77.4±2.1		85.3±2.3	
100	advancing angle	98.9±1.9	0.254	101.3±1.9	0.271	107.0±2.2	0.182
	receding angle	84.3±2.0		85.7±2.0		96.3±2.1	
125	advancing angle	102.9±1.7	0.234	104.7±2.1	0.239	108.9±1.9	0.176
	receding angle	89.4±1.6		90.8±1.8		98.5±2.0	
150	advancing angle	104.6±2.1	0.230	106.1±1.9	0.215	110.5±1.9	0.174
	receding angle	91.3±1.5		93.6±1.6		100.2±1.8	
175	advancing angle	106.6±1.7	0.202	107.3±1.7	0.197	111.3±1.7	0.167
	receding angle	94.8±1.9		95.8±1.6		101.3±1.5	
200	advancing angle	107.0±2.0	0.189	108.0±1.8	0.195	111.0±1.9	0.131
	receding angle	95.9±1.9		96.6±1.7		103.2±1.6	

Table 7-2. Surface tension parameters calculated from the advancing contact angle for Water, Diiodomethane (*DIM*) and Ethylene Glycol (*EG*) on FPTS and FOTS monolayers with the function of anneal temperature.

Process Condition	Contact angles for testing liquid (degrees)			Surface energy(mN/m)			
	Water	E.G.	DIM	γ_s^{LW}	γ_s^-	γ_s^+	γ_s
FOTS monolayers with anneal temperature 23°C	94.2	87.4	93.3	11.28	2.36	1.21	17.01
FOTS monolayers with anneal temperature 150°C	104.6	106.1	110.5	5.35	2.68	0.57	8.41
FPTS monolayers with anneal temperature 23°C	75.9	68.5	79	18.01	3.43	1.61	29.05
FPTS monolayers with anneal temperature 150°C	92.9	98.6	94.9	10.62	3.72	0.11	14.48

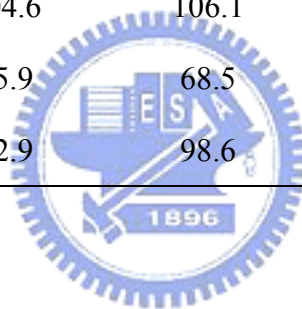


Table 7-3. Surface tension parameters and the advancing contact angle for Water, Diiodomethane (*DIM*) and Ethylene Glycol (*EG*) on FPTs monolayers for immersing in (a) HNO₃ and (b) NaOH solution with concentration of 0.1 N at 100°C as the function of immersion time.

(a)

Immersion time (hr)	Contact angles for testing liquid (degrees)			Surface energy(mN/m)			
	Water	E.G.	DIM	γ_s^{LW}	γ_s^-	γ_s^+	γ_s
0	92.9	98.6	94.9	11.46	2.36	0.64	14.4808
1	92.7	96.4	94.4	11.52	2.68	0.59	14.6824
2	93.2	91.3	93.1	11.32	3.43	0.51	14.8186
3	92.5	89.2	92.6	11.61	3.72	0.44	14.8836

(b)

Immersion time (hr)	Contact angles for testing liquid (degrees)			Surface energy(mN/m)			
	Water	E.G.	DIM	γ_s^{LW}	γ_s^-	γ_s^+	γ_s
0	92.9	98.6	94.9	11.46	2.36	0.64	14.4808
1	92.7	99.9	94.6	11.55	2.11	0.72	14.5884
2	93.0	100.4	94.0	11.41	1.98	0.81	14.6176
3	93.1	101.0	93.6	11.38	1.82	0.89	14.6196

Table 7-4. Surface tension parameters and the advancing contact angle for Water, Diiodomethane (*DIM*) and Ethylene Glycol (*EG*) on FOTS monolayers for immersing in (a) HNO₃ and (b) NaOH solution with concentration of 0.1 N at 100°C as the function of immersion time.

(a)

Immersion time (hr)	Contact angles for testing liquid (degrees)			Surface energy(mN/m)			
	Water	E.G	DIM	γ_s^{LW}	γ_s^-	γ_s^+	γ_s
0	110.5	104.6	106.1	5.35	2.68	0.57	8.4052
1	110.1	102.2	105.2	5.47	2.98	0.54	8.6884
2	111.1	100.2	105.1	5.21	3.32	0.5	8.53
3	110.6	96.6	104.1	5.33	3.82	0.42	8.5388

(b)

Immersion time (hr)	Contact angles for testing liquid (degrees)			Surface energy(mN/m)			
	Water	E.G	DIM	γ_s^{LW}	γ_s^-	γ_s^+	γ_s
0	110.5	104.6	106.1	5.35	2.68	0.57	8.4052
1	110.9	105.5	106.1	5.26	2.54	0.62	8.4096
2	110.1	105.3	105.4	5.48	2.49	0.65	8.717
3	109.6	106.1	105.2	5.6	2.34	0.68	8.7824

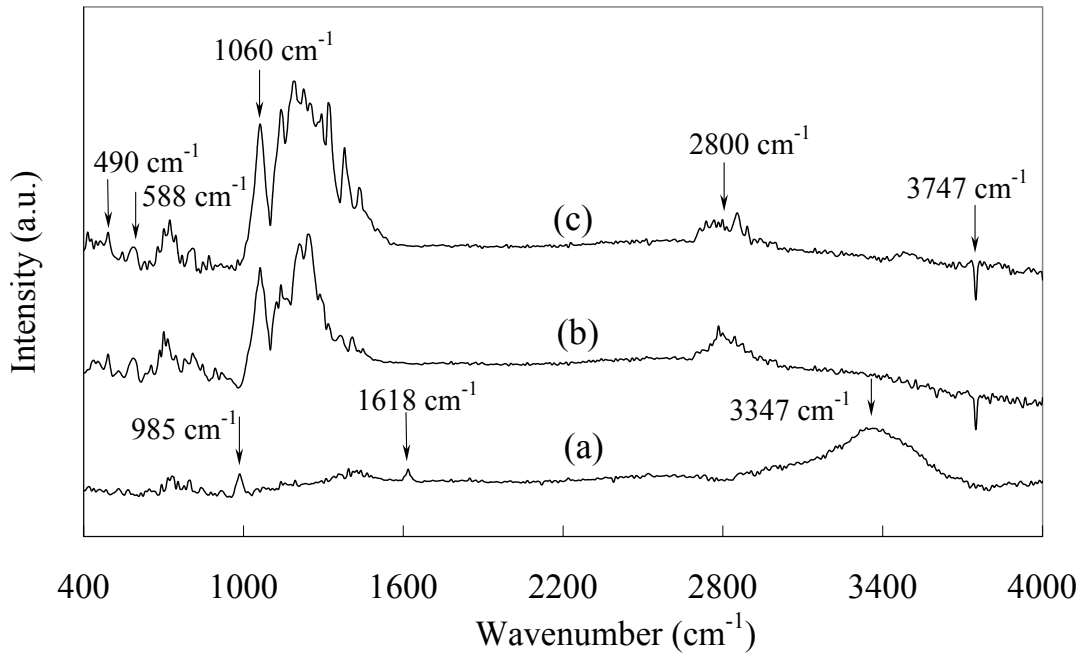


Figure 7-1. FTIR spectra of (a) hydrated silica at room temperature, (b) FOTS and (c) FPTS with the hydrated silica at room temperature following by annealing at 150°C for 2 hours.

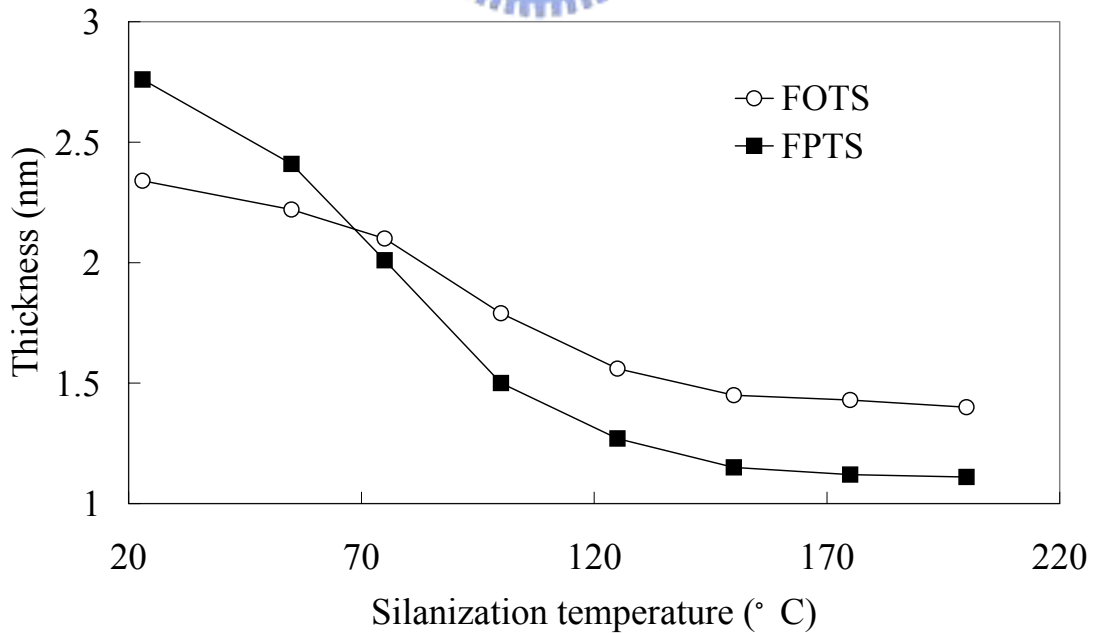
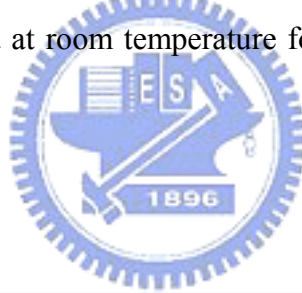


Figure 7-2. Preparation temperature dependence of film thicknesses of SAMs for (a) FPTS and (b) FOTS on silicon oxide substrates.

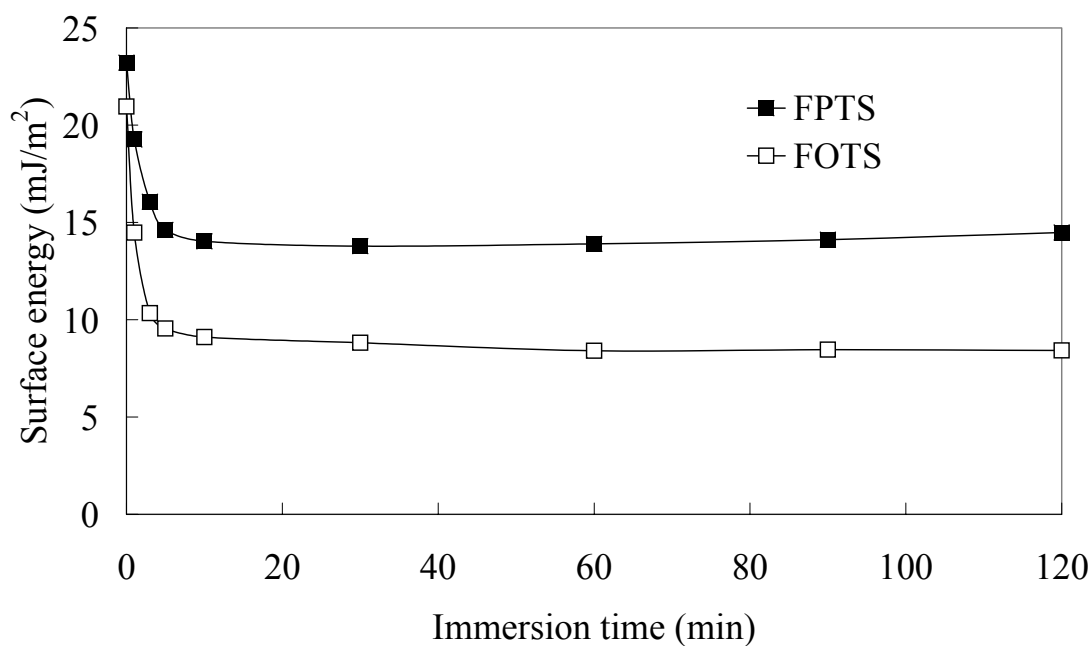


Figure 7-3. Surface energy of FPTS and FOTS monolayers calculated from the contact angles of di-iodomethane, glycol and water as a function of immersion time for monolayers formation.

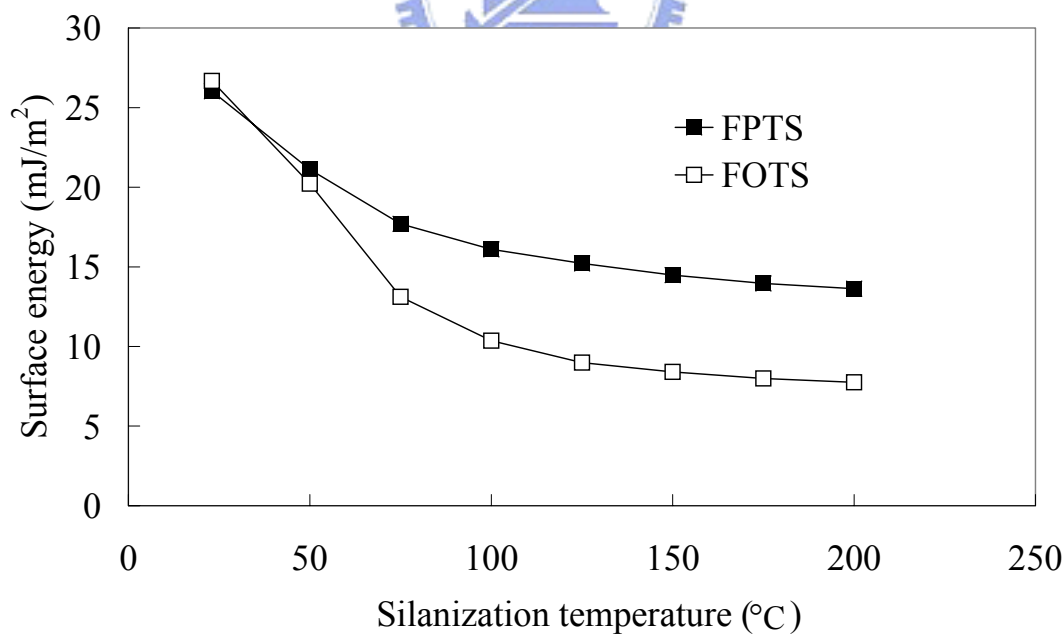
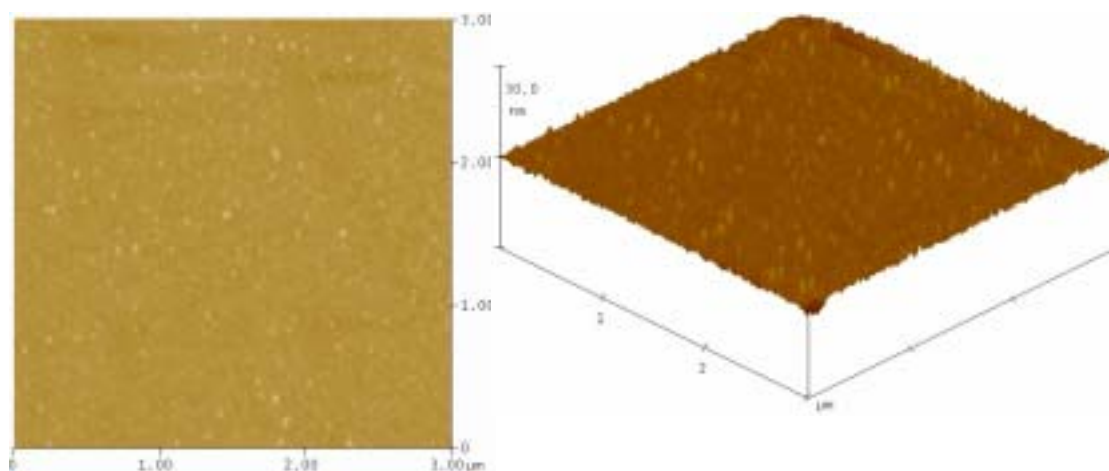


Figure 7-4. Surface energy of FPTS and FOTS monolayers calculated from the contact angles of di-iodomethane, glycol and water as a function of anneal temperature for condensation of self-assembled reaction.

(a)



(b)

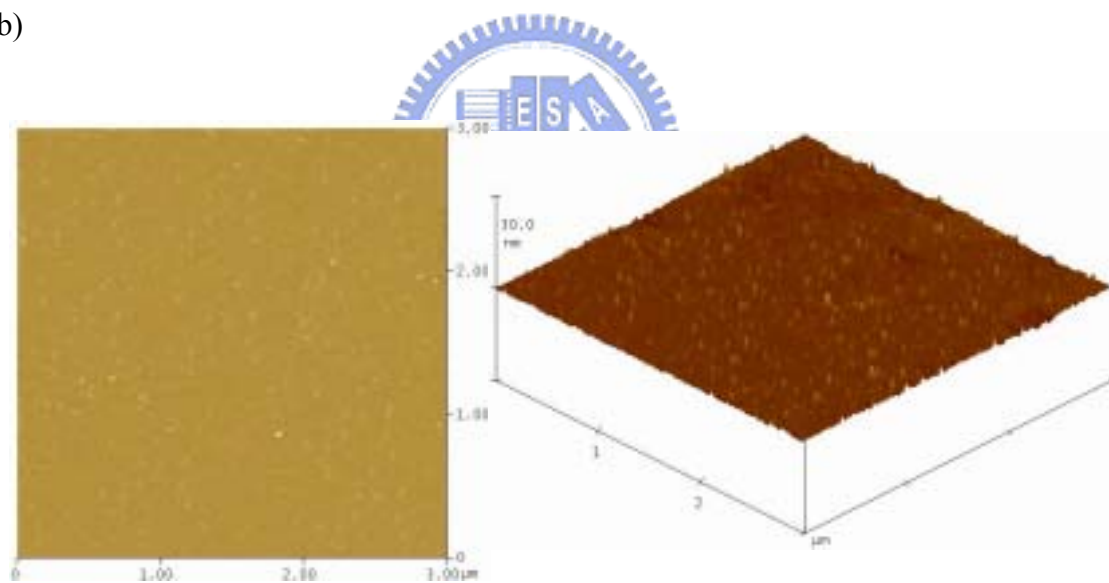
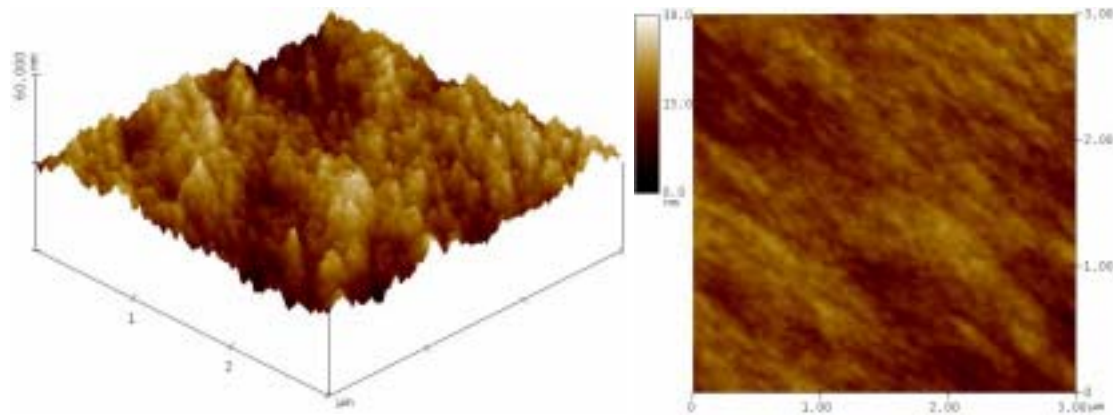
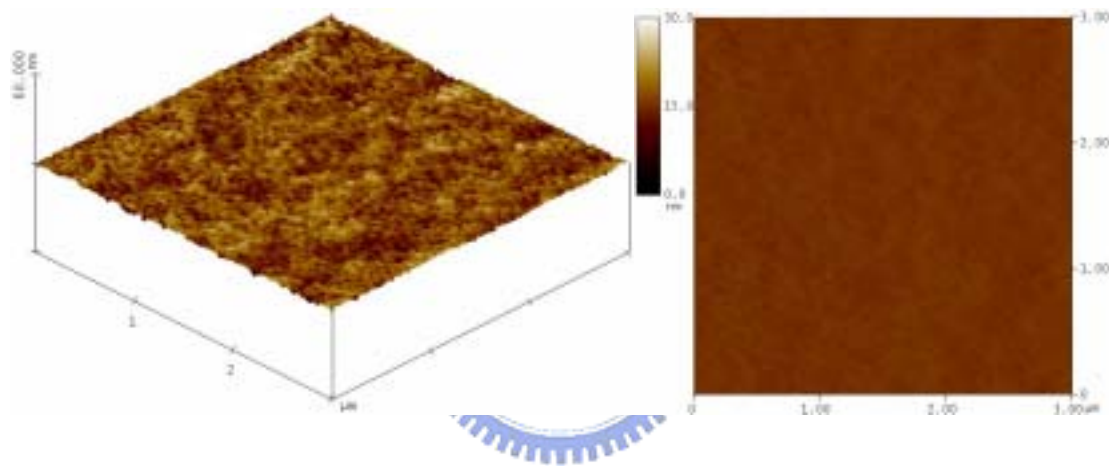


Figure 7-5. AFM images ($1 \mu\text{m} \times 1 \mu\text{m}$) of SAMs for the (a) FPTS and (b) FOTS surface for immersion time of 30 minutes at anneal time of 150°C .

(a)



(b)



(c)

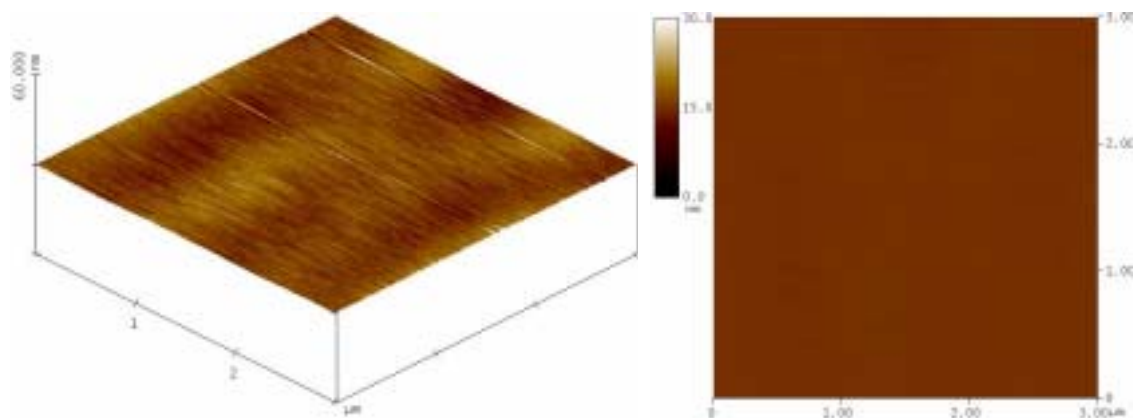
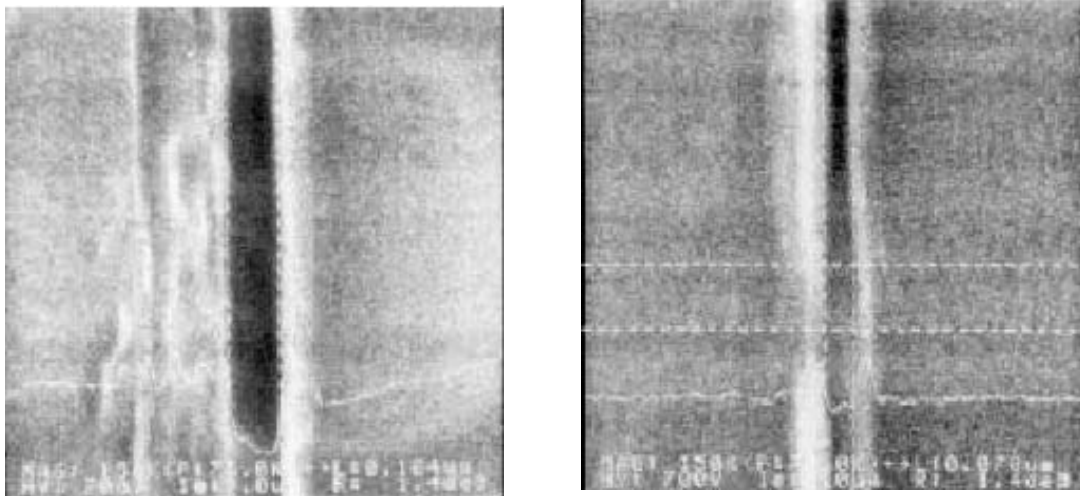
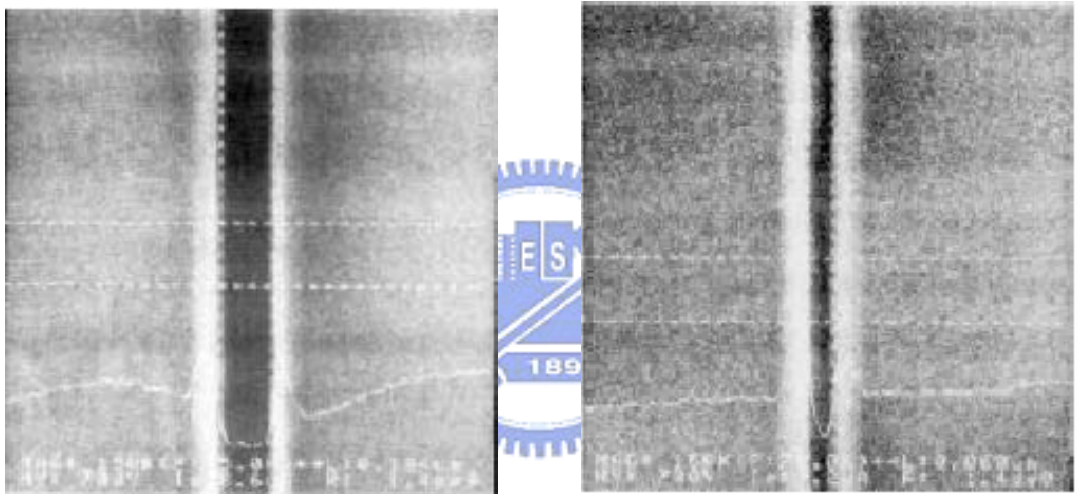


Figure 7-6. AFM images ($1 \mu\text{m} \times 1 \mu\text{m}$) of the resist surface after separated from the mold with the (a) silicon oxide film, (b) FPTS and (c) FOTS SAMs.

(a)



(b)



(c)

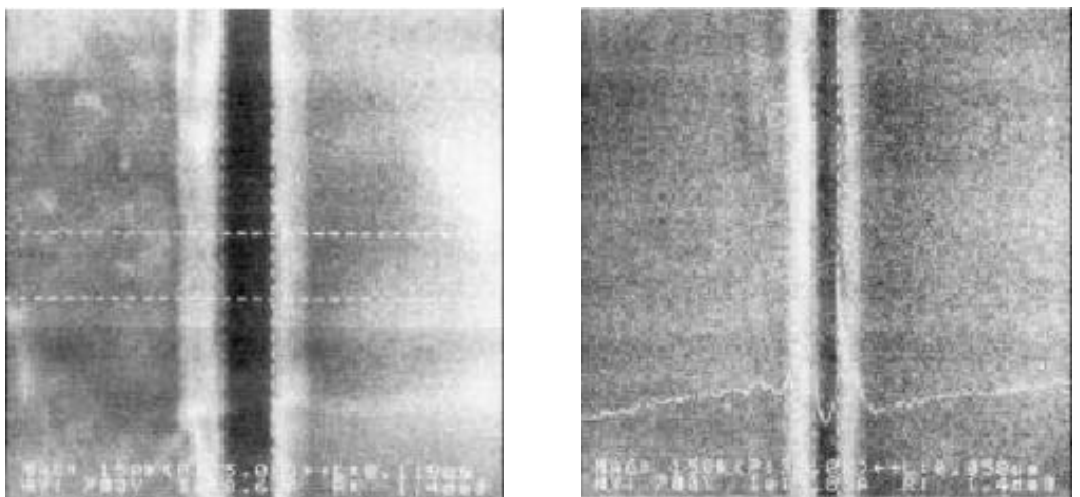


Figure 7-7 SEM images of the iso-trench fabricated by using the mold with the (a) silicon oxide film, (b) FPTS and (c) FOTS SAMs in nanoimprint lithography. The feature sizes of the iso-trench are 120 nm (right) and 60 nm (left), respectively.

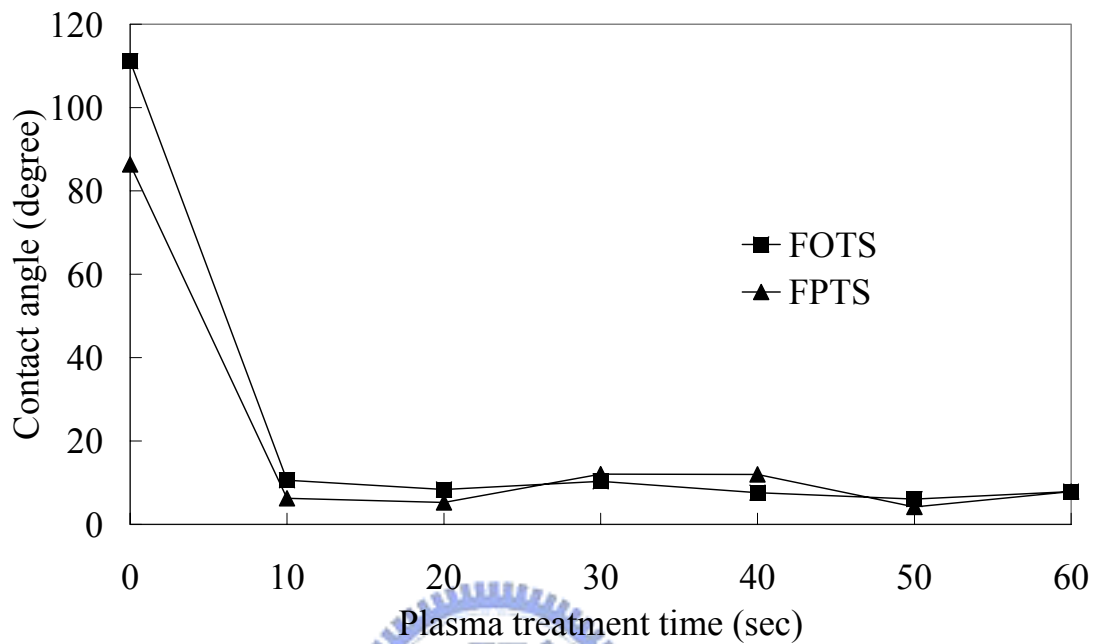


Figure 7-8. The contact angle of water of SAMs for (a) FPTS and (b) FOTS surface treated with oxygen plasma with a series of time.

